ALGORITHMS AND IMPLEMENTATIONS OF APT RESONANT CONTROL SYSTEM[*]

Yi-Ming Wang[†] and Amy Regan, Los Alamos National Laboratory,
P.O. Box 1663, Los Alamos, NM 87545, USA

Abstract

A digital signal processor is implemented to control the resonant frequency of the RFQ prototype in APT/LEDA. Two schemes are implemented to calculate the resonant frequency of the RFQ. One uses the measurement of the forward and reflected fields. The other uses the measurement of the forward and transmitted fields. The former is sensitive and accurate when the operation frequency is relatively far from the resonant frequency. The latter gives accurate results when the operation frequency is close to the resonant frequency. Linearized algorithms are derived to calculate the resonant frequency of the RFQ efficiently using a fixed-point DSP. The control frequency range is about 100kHz for 350MHz operation frequency. A frequency agile scheme is employed using a dual direct digital synthesizer to drive the klystron at the cavity's resonant frequency (not necessarily the required beam resonant frequency) in power-up mode to quickly bring the cavity to the desired resonant beam frequency. This paper will address the algorithm implementation and error analysis, as well as related hardware design issues.

1 INTRODUCTION

Resonant control of the RFQ and superconducting RF cavities requires accurate measurement of the RF cavity resonant frequency. For a digital implementation of the resonant control system in APT/LEDA, an efficient and accurate algorithm is needed to provide a real time error signal to the cavity water cooling system within a desired bandwidth. The algorithm proposed in this paper utilizes the vector measurement of the forward, reflected, and transmitted fields to calculate the complex load impedance or admittance. Knowing the complex load impedance and the loaded quality factor Q of the cavity, the discrepancy of the operating frequency and the resonant frequency can be derived accordingly. A simple linear relationship between the imaginary part of the load admittance and error signal (difference between operating frequency and the cavity resonant frequency) is derived by linearizing a general quadratic relation between the imaginary load admittance and resonant frequency. Numerical simulations reveal that the

difference between the full solution and approximated linear solution is negligible within the frequency range we are interested ($f_0 \pm 100$Hz).

2 SYSTEM IMPLEMENTATION

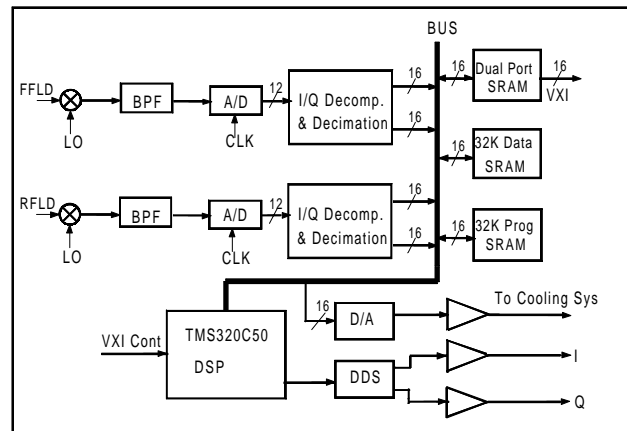Figure 1 is a block diagram of the resonant control module for APT/LEDA.

Figure 1. Block Diagram of Resonant Control Module

The RF frequency is 350MHz for APT/LEDA. The LO is 300MHz. The A/D converter clock is 40MHz. Since the IF frequency is 50MHz, the output of the A/D converter is a data stream consisting of the repeat pattern of measured I, Q, -I, and -Q components. The output of the A/D converter is fed into a multiplexer that switches every other sample into two parallel paths to separate the I and Q components. Then, each channel of the data stream is multiplied by +1 or -1 to remove the alternating sign accordingly. The outputs are the measured I and Q components of the input RF signal. The major advantage of the above described digital I/Q demodulation scheme is the single analog signal path for both I and Q components that ensures a perfect gain-matching between the I and Q signals. Secondly, since the sampled signal is at the IF frequency (50MHz), analog DC offsets and drifts do not affect the accuracy of the digital I/Q demodulation. A dual DDS is used to generate two off-phase error correction sine waves for I/Q modulation in the frequency agile mode.

3 RESONANT CONTROL ALGORITHM

The resonant control algorithm of APT/LEDA is based on the vector measurement of the forward, reflected or transmitted fields. Figure 2 depicts a simplified transmission model for a cavity driven system. The complex load impedance of the cavity is Z_L. The transmission line impedance is Z_0. The forward and reflected field are measured at z_1 and z_2 respectively, which are between $z = 0$ and $z = l$. Here l is the length of the transmission line from klystron to cavity.
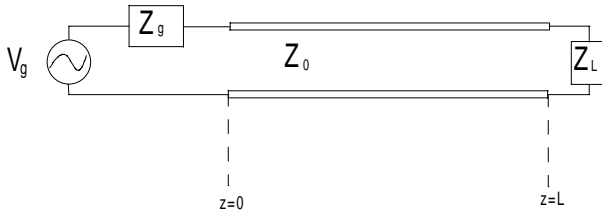

Figure 2. Waveguide with a length of L and load Z_L.

Using the transmission theory[1], we can show that the load impedance is related to the measured forward and reflected fields as

$$Z_L = \frac{V(l)}{I(l)} = Z_0 \frac{V^+(z_1)e^{\gamma(z_1-l)} + V^-(z_2)e^{-\gamma(z_2-l)}}{V^+(z_1)e^{\gamma(z_1-l)} - V^-(z_2)e^{-\gamma(z_2-l)}}$$

(1)

From (1), we have

$$Y_L = \frac{1}{Z_L} = Y_L^r + jY_L^i$$

(2)

For a parallel RLC resonant circuit, Y_L is

$$Y_L = \frac{1}{R}[1 + j(\frac{\omega RC\omega_0}{\omega_0} - \frac{RC}{\omega LC})].$$

(3)

Using $\omega_0 = \frac{1}{\sqrt{LC}}$ and $Q_0 = RC\omega_0$, we have

$$Y_L = \frac{1}{R}[1 + jQ_0(\frac{\omega}{\omega_0} - \frac{\omega_0}{\omega})].$$

(4)

For $Q_0 \gg 0$, and $\frac{|\omega - \omega_0|}{\omega_0} \ll 1$, it can be shown that

$$\omega_0 - \omega = \Delta\omega \approx -\frac{\omega}{2Q_0}\frac{Y_L^i}{Y_L^r}$$

(5)

Eq. (5) is used to determine the difference between the resonant frequency and the operation frequency.

4 SIMULATION RESULTS

To verify the validity of the algorithm, a simulation was conducted using Eq. (5) and Eq. (1) to get the error signal vs. Frequency with a random noise added to the measured fields(20dB Signal-to-Noise Ratio). The results are shown in Figure 3. This result shows that Eq. (5) together with Eq. (1) gives a satisfactory result within the frequency range we are interested.
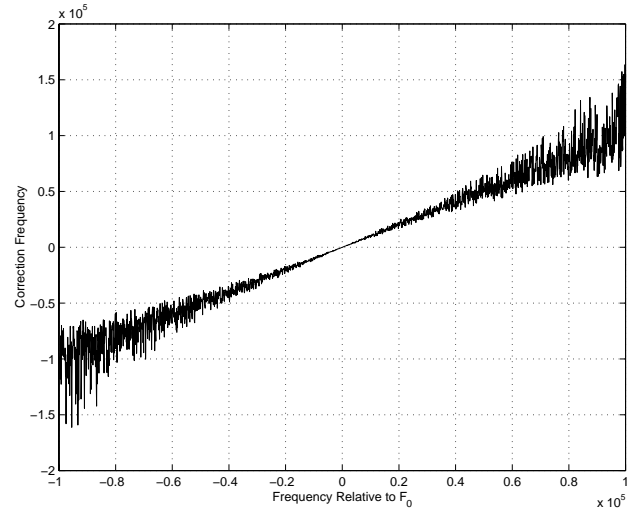

Figure 3. The result with noise in the measurement.

In figure 3, the correction frequency is obtained when the SNR (Signal-to-Noise Ratio) of the measured field is 20dB. Notice that the perfect gain-matching in our digital I/Q demodulation scheme ensures the equal effect of noise on both I and Q channels. Thus, we can represent the measured field as $(1 + r)F$, where r is noise, F is the complex field without noise. Mathematically, this means that the noise correlation coefficient between two channels (I and Q) is one.

One important feature in Figure 3 is that the correction frequency never crosses zero on both sides of the resonant frequency f_0. This indicates that no ambiguity can exist regarding the sign and/or direction the correction frequency required. Next we investigated the correlated and uncorrelated I/Q noise on robustness of the algorithm. Here, we assumed that the SNR of the measurement is only 3dB. Figure 4 is for a completely correlated noise case. Figure 5 is for a completely uncorrelated noise case. It is very important to notice that the correction frequency never crosses zero on both sides of the resonant frequency for the case with the completely correlated noise for I/Q components. This means that when we implement this algorithm in this case, we always have a correct sign for the error signal. In contrast, the correction signal for the completely uncorrelated case back does across zero on both sides of the resonant frequency, potentially leading to ambiguity.

As mentioned before, the digital I/Q decomposition scheme implemented in our system ensures the perfect gain-matching for the I and Q channels which results in the completely correlated noise for the I and Q channels.

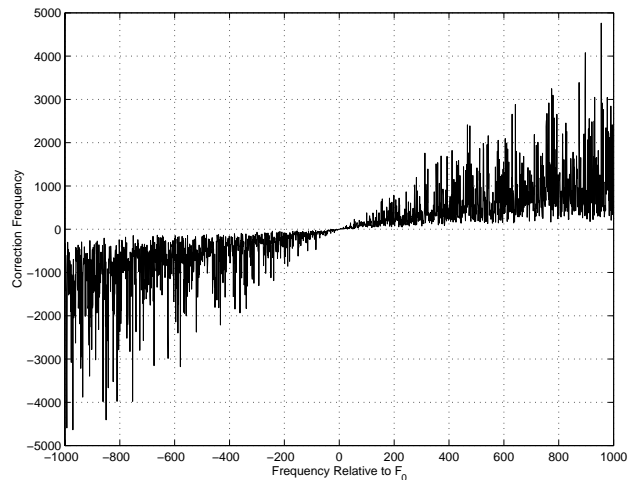Therefore, the algorithm applied to our system is very robust.

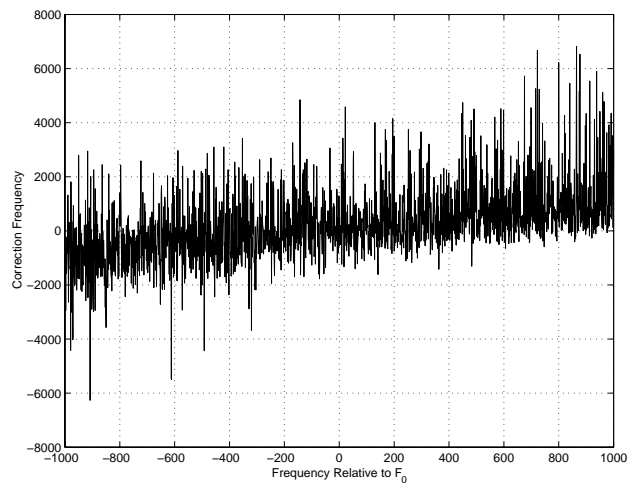Figure 4. Result for the correlated noise case.

Figure 5. Result for the uncorrelated noise case.

5 OTHER CONSIDERATIONS

Here, all formulas are derived based on the forward and reflected fields. Similar formulas can also be derived from the forward and transmitted fields. Mathematically, they are equivalent. But some practical issues should be addressed when we decide which set of formulas to use in the system implementation. One limitation comes from the finite resolution of the A/D converter. For a 12bit A/D converter, as used in our system, the dynamic range of measurement is around 60dB. However, due to some instrumentation limitations, such as isolation of the directional coupler, the dynamic range of the measured signal could be 10 to 20 dB lower than the theoretical dynamic range of the A/D converter. Given the above consideration we don't want the magnitude of the

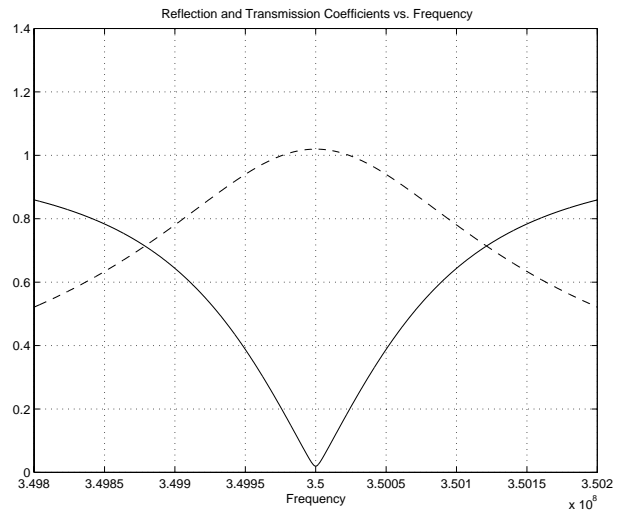measured field to change dramatically during normal operation.

Figure 6. Magnitude of the reflection and transmission coefficients vs. frequency.

Figure 6 depicts the magnitude of the reflection and transmission coefficients for an equivalent RLC load with $Q = 3000$ and $f_0 = 350$ MHz. From Figure 6, we can see that using the reflected field algorithm is good when the frequency is relatively far from resonance but the accuracy of the measurement will deteriorate when the frequency is close to resonance. However, on the other hand, the accuracy of the transmitted field algorithm is higher when the frequency is close to resonance and lower when the frequency is away from resonance. Based on the above observation, both algorithms are implemented in our system. The reflected field algorithm will be activated when the frequency is relatively far from resonance and the transmitted field algorithm will be activated when the frequency is close to resonance.

6 CONCLUSIONS

An efficient and simple algorithm that is suitable for the implementation in a digital signal processor is proposed. The simulation results reveal that the algorithm is very robust when implemented with the digital I/Q demodulation scheme used in our system. The algorithm gives a good result with a noise level at 20dB SNR.

REFERENCES

[1] Cheng, K.C., 'Field and Wave Electromagnetics', Second Edition, Addison-Wesley, 1989.

[2] Ziomek, C. and Corredoura, P., 'Digital I/Q Demodulator', PAC'95, 1995.